Matter

CellPress

Article

Complete deciphering of the dynamic stereostructures of a single aggregation-induced emission molecule

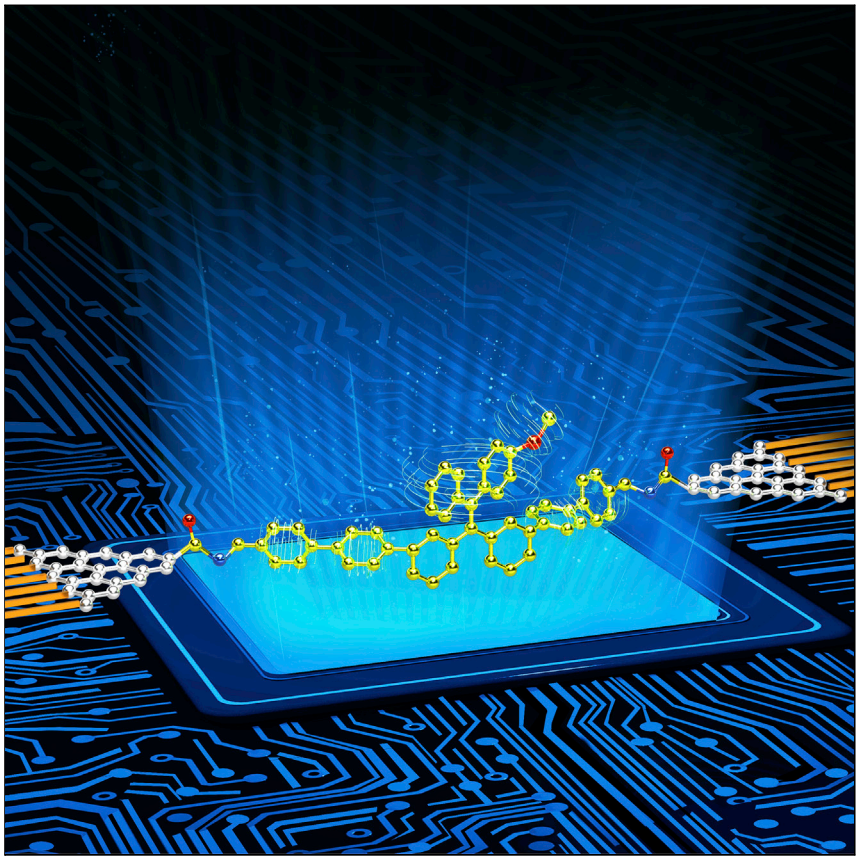

Caiyao Yang, Pingchuan Shen, Qi Ou, ..., Zhigang Shuai, Ben Zhong Tang, Xuefeng Guo

zgshuai@tsinghua.edu.cn (Z.S.)
tangbenz@cuhk.edu.cn (B.Z.T.)
guoxf@pku.edu.cn (X.G.)

Highlights

Accurate detection and deciphering of single-molecule dynamic stereostructures

Recognition of intramolecular motions with single bond resolution

Regulation of C=C bond isomerization via temperature and electric field

A deep understanding of the dynamic structure-property relationship is crucial to functional molecular devices. This article reports a reliable cutting-edge method to construct single-molecule devices by integrating tetraphenylethylene (TPE)-based derivatives into graphene nanogaps via covalent bonds, leading to *in situ* long-time conductance measurements in real time. This method enables unambiguous recognition of intramolecular motions and complete deciphering of single-molecule dynamic stereostructures, thus providing new insights into the development of practical applications of ultra-sensitive devices.

Understanding
Dependency and conditional studies on material behavior

Yang et al., Matter 5, 1–11
April 6, 2022
https://doi.org/10.1016/j.matt.2022.01.016

Please cite this article in press as: Yang et al., Complete deciphering of the dynamic stereostructures of a single aggregation-induced emission molecule, Matter (2022), https://doi.org/10.1016/j.matt.2022.01.016

Matter

CellPress

Article

Complete deciphering of the dynamic stereostructures of a single aggregation-induced emission molecule

Caiyao Yang,[1,2,7] Pingchuan Shen,[1,7] Qi Ou,[3,7] Qian Peng,[4,7] Shuyao Zhou,[2] Jinshi Li,[1] Zhirong Liu,[2] Zujin Zhao,[1] Anjun Qin,[1] Zhigang Shuai,[3,*] Ben Zhong Tang,[1,5,*] and Xuefeng Guo[2,6,8,*]

SUMMARY

The realization of functional molecular devices is inseparable from deep understanding of the intrinsic structure-property relationship of molecules. However, due to limited detection sensitivity and temporal resolution of current methods, there are rare reports on fully probing *in situ* dynamic changes of the molecular stereostructures at the single-molecule level in real time. Here, we present a complete deciphering of the dynamic stereostructures of a single aggregation-induced emission molecule using molecular junctions, which are capable of executing rapid real-time electrical measurements to achieve the unprecedented electrical mapping, thus feeding back the dynamic changes of the molecular stereostructures. Experimental and theoretical investigation consistently verify the intramolecular motions under electric field and the isomerization dynamics with strong temperature and electric field dependence, offering new insights into the development of ultra-sensitive devices. We anticipate that further integration of optical measurements with this approach will enable sophisticated synchronous monitoring of broad single-molecule photochemistry and photophysics.

INTRODUCTION

Revealing the dynamic change of single-molecule stereostructures is crucial to the discovery and understanding of fundamental physical phenomena and novel effects of materials at the atomic or molecular level that are not accessible using traditional approaches, and provides guidance for the design of future molecular electronic devices.[1] Any subtle perturbation of molecular geometry may induce a significant change of the molecular properties, setting the basis for designing and creating practical molecular devices.[2–10] At present, research on external gating to regulate the performance of molecular devices is in full swing,[11–13] most based on the occurrence of chemical reactions (photocyclization[14,15] *trans-cis* isomerization,[16] tautomerization,[17,18] etc.) owing to the evident changes of electronic and geometric structures. The configurational or conformational changes of molecules have been used to build switching and rectification functions[19–22] as well as control quantum interference effects.[23–25] However, it is particularly difficult to detect the dynamic conductance changes in the case of single bond rotation that induces no significant structural change. Because previous ensemble experiments proved that the time range of single bond rotation is from femtoseconds to nanoseconds,[26,27] it is a formidable challenge for ordinary electrical experimental methods to obtain a distinct signal while satisfying high temporal resolution. In addition, the interfacial contact stability of molecular devices constructed by non-covalent bonding is worse,

Progress and potential

Capturing the dynamic change of single-molecule stereostructures is crucial to understanding the underlying mechanisms of fundamental physical phenomena and novel effects. However, due to limited detection sensitivity and temporal resolution of traditional measurements, it is a formidable challenge to detect delicate molecular stereostructures at the single-molecule level in real time.

Here, we report a single-molecule electrical methodology to achieve the unprecedented electrical mapping, thus feeding back the fine dynamic change of the molecular stereostructures. This method succeeds in completely deciphering the dynamic stereostructures of a single aggregation-induced emission molecule, and is mature to be applied immediately to make complex synchronous monitoring possible in combination with the optical technology, holding great promise for the development of a multimodal single-molecule detection platform capable of discovering unexpected phenomena and enriching new chemistry.

resulting in larger current fluctuations, which makes it more difficult to observe the small conductance changes caused by intramolecular motions. To solve these issues, we connected the designed molecule to nanoscale graphene point electrodes via covalent amide bonds, ensuring only one-molecule connection and avoiding the intermolecular interaction that affects the charge transport properties. As graphene is more compatible with organic molecules than metals, the genuine molecular structural information can be more precisely reflected via the corresponding conductance of molecular junctions. In addition, temperature is essentially a measure of relative atomic or molecular motions. Exploring reactions under extreme cooling has nonetheless been a research focus.[28–30] Coupled with the restriction effect of a fixed molecule and the cryogenic environment, the molecular motion behavior can be slowed down to a certain extent to meet the requirement of electrical measurements.

In this work, we have witnessed great potentials of using graphene-molecule-graphene single-molecule junctions (GMG-SMJs) as an electrical platform for revealing the dynamic process of molecular stereostructures at the single-molecule level. Through molecular engineering, we designed and synthesized three tetraphenylethylene (TPE)-based derivatives (named TPE-2A, OTPE-2A, and TPE-OME-2A), and embedded them into nanogapped graphene point electrodes by forming covalent amide bonds to construct GMG-SMJs (Figures 1A, 1B, and S1). Details of the molecular synthesis and device fabrication are provided in the Experimental procedures section and the supplemental information (Figures S1 and S2). As a family of the prototypical aggregation-induced emission (AIE) compounds, TPE and its derivatives have been widely studied and applied in multiple disciplines.[31,32] Tremendous experimental and theoretical studies[33–35] have shown that the presence of intramolecular motions associated with non-radiative relaxation in TPE molecules, such as C=C twisting, phenyl rotation, and formation of a photocyclized intermediate, leads to the reduction of the fluorescence quantum yield of the materials in non-rigid environments (e.g., dilute solution or gas phase). Therefore, in-depth understanding of these intramolecular motions is of critical importance to thoroughly expose the AIE mechanism and the development of new AIE materials. On the basis of previous reports,[33,36] we hypothesize that molecules fixed in the graphene nanogap might exhibit four kinds of molecular motions: (1) C=C bond twisting of TPE; (2) phenyl rotation of TPE; (3) cyclization of TPE; and (4) biphenyl torsion at both ends of the molecular bridge. Remarkably, the elaborate dynamic behaviors of these stereostructural transitions can be distinguished through accurate measurements of the sequential multilevel molecular conductance at cryogenic temperatures.

Figure 1A depicts a schematic diagram of GMG-SMJs constructed with one of the molecules mentioned above. The successful fabrication of GMG-SMJs is determined by testing whether a closed loop is formed after connecting the molecules between the source and the drain electrodes (Figures S2 and S3). Furthermore, we performed inelastic electron tunneling spectroscopy (IETS) and assigned the observed spectral features to specific molecular vibrations in comparison with the theoretical infrared and Raman spectra (Figure 1C; another set of data is provided in Figure S4). Figures 1D and 1E show the validation of the high-resolution IETS measurements with AC modulation voltage and temperature dependence, which were carried out according to a previously reported method.[37,38] When the modulation voltage or temperature increases, the two peaks representing δ(C−H)(Ar) and ν(C−O)(Ar) gradually merge into one peak and finally become flat. Correspondingly, the full width at half maximum of the peak obtained by Gaussian fitting shows a trend of becoming wider. These evidences concordantly demonstrate that this single-molecule

[1]State Key Laboratory of Luminescent Materials and Devices, Guangdong Provincial Key Laboratory of Luminescence from Molecular Aggregates, SCUT-HKUST Joint Research Institute, AIE Institute, Center for Aggregation-Induced Emission, South China University of Technology, Guangzhou 510640, P. R. China

[2]Beijing National Laboratory for Molecular Sciences, National Biomedical Imaging Center, College of Chemistry and Molecular Engineering, Peking University, Beijing 100871, P. R. China

[3]MOE Key Laboratory of Organic OptoElectronics and Molecular Engineering, Department of Chemistry, Tsinghua University, Beijing 100084, P. R. China

[4]School of Chemical Sciences, University of Chinese Academy of Sciences, Beijing 100049, P. R. China

[5]Shenzhen Institute of Molecular Aggregate Science and Engineering, School of Science and Engineering, The Chinese University of Hong Kong, Shenzhen, 2001 Longxiang Boulevard, Longgang District, Shenzhen City, Guangdong 518172, P. R. China

[6]Center of Single-Molecule Sciences, Frontiers Science Center for New Organic Matter, Institute of Modern Optics, College of Electronic Information and Optical Engineering, Nankai University, 38 Tongyan Road, Jinnan District, Tianjin 300350, P. R. China

[7]These authors contributed equally

[8]Lead contact

*Correspondence: zgshuai@tsinghua.edu.cn (Z.S.), tangbenz@cuhk.edu.cn (B.Z.T.), guoxf@pku.edu.cn (X.G.)

https://doi.org/10.1016/j.matt.2022.01.016

Please cite this article in press as: Yang et al., Complete deciphering of the dynamic stereostructures of a single aggregation-induced emission molecule, Matter (2022), https://doi.org/10.1016/j.matt.2022.01.016

CellPress

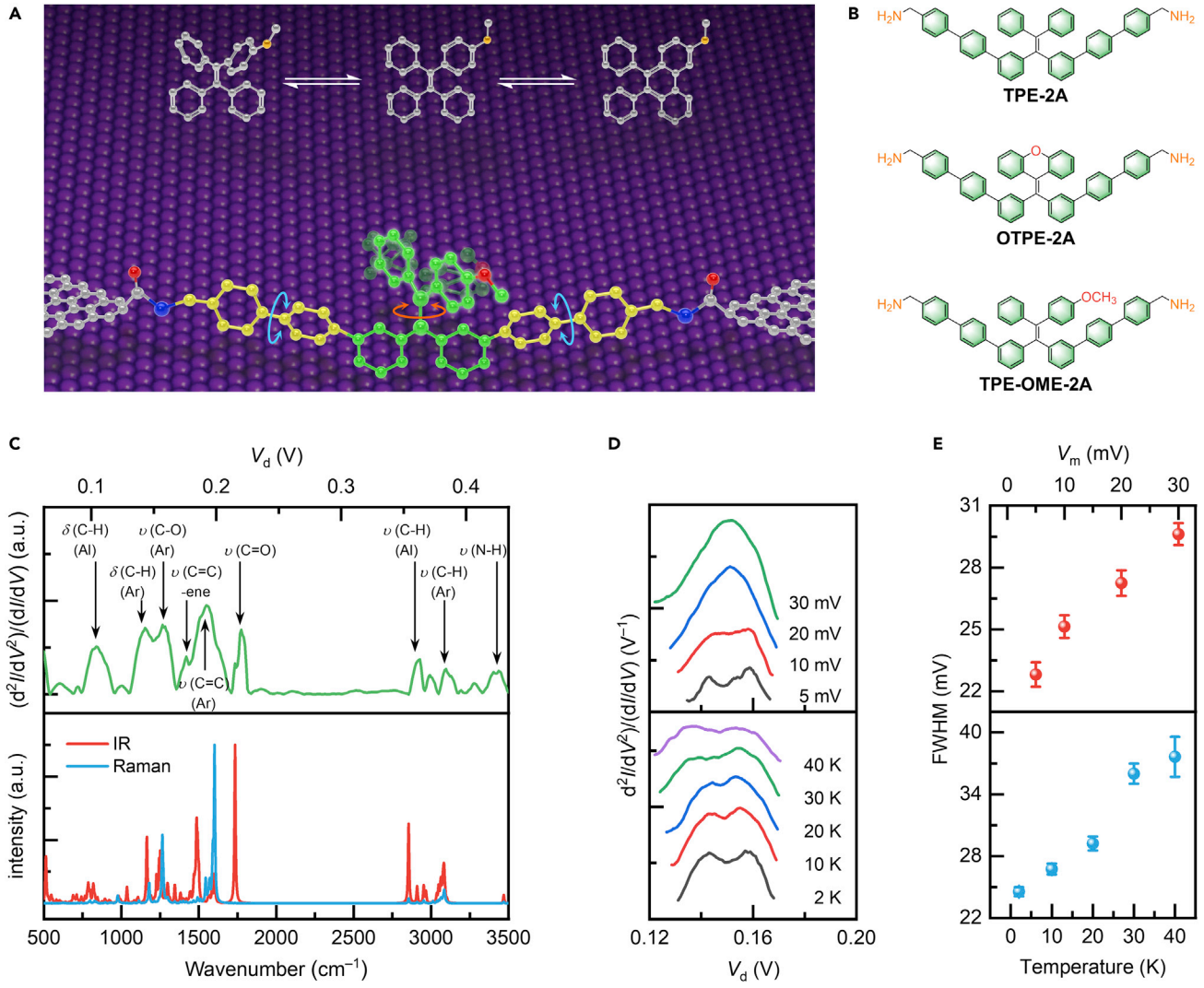

Figure 1. Device structure and electrical characterization of GMG-SMJs

(A) Schematic representation of the device structure that highlights the detection of single-molecule dynamic stereostructures via molecular conductance measurements.

(B) Molecular structures of three TPE-based derivatives (TPE-2A, OTPE-2A, and TPE-OME-2A).

(C) Top: high-resolution IETS for molecular junctions (formed from TPE-OME-2A) measured by a lock-in second-harmonic technique at 2.0 K with an AC modulation of 10.6 mV (rms value) at a frequency of 233 Hz. Bottom: corresponding calculated infrared and Raman spectra.

(D) Successive IETSs for the δ(C−H)(Ar) and ν(C−O)(Ar) modes with AC modulation voltage (top) and temperature (bottom) dependence.

(E) The trend of full width at half maximum (FWHM) of the peaks with increasing the AC modulation voltage (top) and temperature (bottom). The error bars are determined by the Gaussian fittings. A constant temperature of 2.0 K is used for voltage-dependent experiments and a fixed voltage of 10.6 mV is used for temperature-dependent experiments.

electrical method can capture various motions of a single molecule, precluding the possibility that the experimental data are influenced by two or even more molecules.

RESULTS AND DISCUSSION

Real-time electrical measurements and conductance attribution

It is well known that the electronic and geometric structures of molecules are closely related to molecular conductance.[39] To better establish the relationship between the molecular structure and the conductance state, we performed real-time current

Please cite this article in press as: Yang et al., Complete deciphering of the dynamic stereostructures of a single aggregation-induced emission molecule, Matter (2022), https://doi.org/10.1016/j.matt.2022.01.016

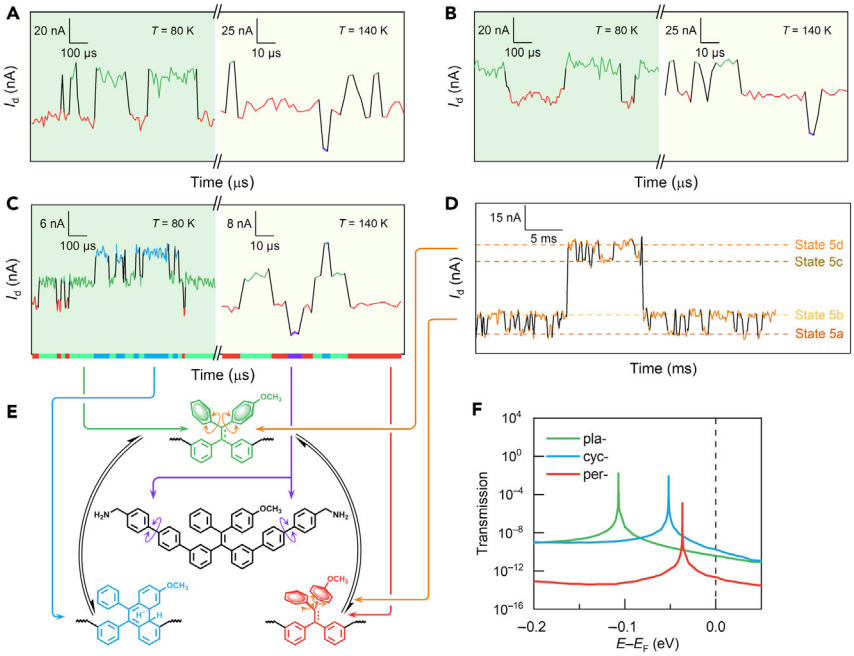

Figure 2. Intuitive feedback of current signals to intramolecular motions

(A–C) Representative current trajectories of single-molecule junctions connected with TPE-2A (A), OTPE-2A (B), and TPE-OME-2A (C), respectively, at 80 K (light green background) and 140 K (light yellow background). The trajectories marked with different colors represent a certain metastable conformation or structure during the molecular motion.

(D) Representative current trajectories of a device connected with TPE-2A at 10 K. The trajectories marked in yellow emphasize the phenyl rotation.

(E) Schematic diagram of the main transformation process and the attribution of the corresponding conductance states as shown in (A–D).

(F) Transmission spectra of the three structures or conformations in Figure 4E. According to the transmission coefficients at the Fermi level of graphene, the conductance sequence from high to low is the cyclization structure (blue curve), the quasi-planar conformation (green curve), and the perpendicular structure (red curve), respectively.

(*I*–*t*) measurements of the devices connected with three different molecules at different temperatures, ranging from 80 to 160 K (Figures S5–S7; Tables S1–S3). To avoid the damage of a high bias voltage to the device and the weak conductance change when the bias voltage is too low, we optimized the bias voltage to be 300 mV, ensuring the stability and reliability of the devices as well as a high signal-to-noise ratio. Figures 2A–2C are the representative *I*–*t* trajectories of the devices connected with TPE-2A, OTPE-2A, and TPE-OME-2A, respectively, which were randomly selected at 80 K (light green background) and 140 K (light yellow background). It is clear that, when the temperature is below 140 K, the *I*–*t* curves of the device connected with OTPE-2A are basically similar to those of TPE-2A, with two salient conductance states (labeled as State 1 and State 2, and marked in red and green, respectively). However, a higher conductance state (State 3 marked in blue) only appears in electrical signals of the device connected with TPE-OME-2A. When the temperature increased to 140 K, a new conductance state with a low percentage (State 4 marked in purple) was detected in the *I*–*t* curves, which can be observed in all the devices connected with these three molecules, except for the different switching frequency of the conductance states. Note that inside these obvious conductance states, there are also small persistent current fluctuations (only noticeable at lower temperatures, as shown in Figures 2D and S8) with high-frequency and short lifetime features.

Please cite this article in press as: Yang et al., Complete deciphering of the dynamic stereostructures of a single aggregation-induced emission molecule, Matter (2022), https://doi.org/10.1016/j.matt.2022.01.016

Figure 2E completely reveals the sequential and multilevel changes of single-molecule stereostructures, taking the TPE-OME-2A molecule as an example. By comparing the three molecular structures and the characteristics of the current signals, we assume that States 1 and 2 originate from the central quasi C=C bond twisting excited by the electric field. State 3, from the device connected with TPE-OME-2A, can be converted only from State 2 and the current level is relatively higher, which suggests that this conductance state may be related to the formation of a new chemical structure rather than the rotation of the anisole or benzene ring, such as the cyclized intermediate. The molecular structures marked in red, green, and blue represent the perpendicular conformation, quasi-planar conformation, and instantaneous cyclization structure in the twisting process of the double bond under the action of electric field, respectively. The transformation relationship between these structures corresponds well to the time sequence of the above conductance states. In addition, the transmission spectrum (Figures 2F and S9) and the theoretical calculated $I-V$ curves (Figure S10) further confirm the conductivity sequence of the three structures, which is consistent with our conjecture. Although the perturbed highest occupied molecular orbital (*p*-HOMO) of the perpendicular conformation is the closest to the Fermi level of graphene, it has the smallest peak value, thus leading to the lowest state. State 4 appears at higher temperatures; a similar phenomenon was observed in our previous work.[36] We suppose that this is caused by the torsion between the functional core and the biphenyl at both ends of the molecular junction, and this movement can only be activated above an effective temperature threshold.

Through the above analysis, we attributed the small persistent current fluctuation with spike-like features to the phenyl rotation of TPE, which is relatively difficult to identify because of its extremely fast rotation speed at high temperatures and small conductance change. Notably, two distinct conductance states (State 1 and State 2) that are caused by C=C bond twisting are clearly accompanied by smooth current fluctuations at 10 K (labeled as States 5a–5d, according to the order of conductance from low to high, and marked in different shades of yellow in Figures 2D and S8), which intuitively displays the step-by-step and sequential process of the phenyl rotation. In comparison with the previous test results at higher temperatures, there are no longer high-frequency and short lifetime current signals, but a stepped feature, due to the lower ambient noise in the test chamber at low temperatures. We separated the current signals representing State 1 and State 2 and idealized them into a four-level interconversion (Figure S11). Finally, we deduced that the average lifetimes of States 5a–5d were all around 120 μs (Figure S12), confirming that they indeed originate from the same motion behavior, namely, the phenyl rotation.

Theoretically, we first unravel the mechanism of the transformation between various conductance states in Figure 3A. The metastable structures of three conductance states are optimized and visualized as shown in Figure 3A, together with their relative energies. Since the biphenyl rings are not responsible for the transition between the three conductance states mentioned above, for simplicity we only investigated the functional core (which excludes the biphenyl rings) in Figure 3A. The schematic potential energy curves that connect these structures are also depicted. It can be seen that the transformation between the quasi-planar and perpendicular conformations is indeed initiated by the formation of the triplet states under electrical excitation. Note that the possibility of forming triplet excitons under electrical excitation is three times the possibility of forming singlet excitons based on spin statistics,[40] and the rate of forming triplet excitons is comparable with that of forming singlet

Please cite this article in press as: Yang et al., Complete deciphering of the dynamic stereostructures of a single aggregation-induced emission molecule, Matter (2022), https://doi.org/10.1016/j.matt.2022.01.016

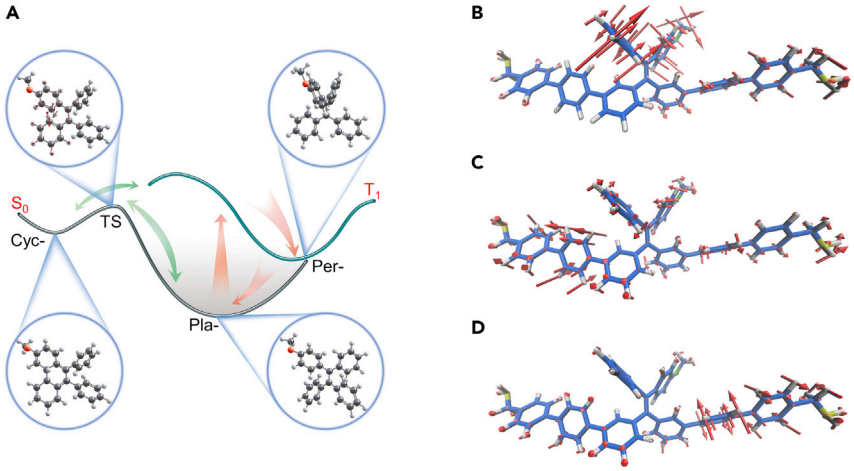

Figure 3. Theoretical explanation of each conductance state

(A) The transformation mechanism between different conductance states.

(B–D) Essential normal modes that trigger the transformation between different conductance states at the optimized geometry of the quasi-planar conformation.

excitons due to the fact that this is a direct excitation process rather than a normal intersystem crossing process triggered by spin-orbit coupling. After being excited to the triplet state, the optimized ground state structure of the functional core, which is quasi-planar, converts to a perpendicular conformation, which is actually the optimized structure of the triplet states. At such a perpendicular conformation, the triplet state is energetically degenerate with the singlet state, making it possible for an efficient transformation to the quasi-planar conformation. On the contrary, the transformation between the quasi-planar conformation and the cyclization structure takes place via a transition state, of which the vibrational mode with the imaginary frequency is also visualized in Figure 3A. It can be seen that such a mode indicates the directions of two metastable states. Note that the cyclization structure lies higher in energy in comparison with the quasi-planar and perpendicular conformations, which is consistent with the fact that the proportion of State 3 is smaller than that of State 2 and State 1, as experimentally observed. Additional metastable conductance states arise from the torsion of the biphenyl rings in TPE-OME-2A, which were detected and analyzed in our previous work.[36] The transformation of these conformations also takes place via corresponding transition states, which are visualized in Figure S13 together with the modes of the imaginary frequency.

Next, we provide a detailed analysis of the temperature dependence of each conductance state based on normal mode analysis at the optimized geometry of the quasi-planar conformation of TPE-OME-2A. Essential normal modes that are responsible for the switching between various optimized ground state structures are theoretically investigated and visualized in Figures 3B–3D. These essential normal modes, including the phenyl rotation that connects the quasi-planar conformation and cyclization structure (Figure 3B), and the biphenyl torsion on the side benzene rings (Figures 3C and 3D), can effectively trigger the transition between different conductance states. Note that the transformation between the quasi-planar and perpendicular conformations takes place via the spontaneous vibrational relaxation after electrical excitation, which is consistent with the experimental observation that both the quasi-planar and perpendicular conformations can be detected at low temperatures after applying an electric field. The phenyl rotation mode, with a frequency at 62.51 cm^{-1}, corresponds to ~89.94 K in temperature and is in line with

the experimental observation that the transformation from the quasi-planar conformation to the cyclization structure is detected at around 80 K. The frequencies of two biphenyl torsion modes, 84.68 and ~85.41 cm^{-1}, correspond to a higher temperature around 140 K, which makes it possible to detect additional conductance states at 140 K under an electric field. Note that the transition between two given conformations is indeed determined by their energy barrier, which can be presumably overcome via electrical excitation. The good agreement between the corresponding temperature of these essential modes and the experimental observation indicates that the thermal excitation of a given mode is a necessary but not sufficient precondition to initiate the transition between two metastable conformations that are connected by this mode.

The reason why no cyclization structure has been captured for TPE-2A, which is in distinct contrast to TPE-OME-2A, is schematically explained in Figure S14. Our theoretical calculations demonstrate that the cyclization structure of TPE-OME-2A corresponds to a ground state local minimum, while that of TPE-2A corresponds to a minimum-energy crossing point (MECP) between the ground and the excited state according to theoretical investigation via spin-flip time-dependent density functional theory,[41] which is an unstable structure and is expected to quickly decay to the optimized planar structure. This cyclization MECP structure for TPE has been reported previously[42] with different levels of electronic structure theory. In TPE-OME-2A, the cyclization structure is considerably stabilized due to the electron-donating ability of methoxy group and hence becomes a local minimum of the ground state that can be detected experimentally.

Temperature-dependent measurements

Since the traces of C=C bond twisting can be captured in a relatively large temperature range, we have meticulously studied the typical behavior of this kind of intramolecular transition. Representative temperature-dependent and voltage-dependent $I-t$ curves are presented in Figures 4A and 4B, respectively. Figure 4A represents the real-time $I-t$ curves and corresponding current distribution histograms of the device connected with TPE-2A at different temperatures ranging from 10 to 80 K. We observed that there are two distinct conductance states (States 1 and 2) in $I-t$ curves, which are marked in red and green, respectively, in the current distribution histograms. Reproducibly, the small persistent current fluctuations within States 1 and 2 originating from the phenyl rotation of TPE were also observed at each temperature. The lower the temperature, the clearer the signals become. To analyze the dynamics of the stereostructures, especially the quasi C=C bond twisting, current signals in $I-t$ trajectories were idealized into a two- or four-level interconversion by using QuB software (Figure S11). The average lifetime of each conductance state can be derived from the plots of the dwell time of corresponding states, which could be well fitted by a single-exponential function (Figure S15). We calculated the area of the current distribution histograms and obtained the proportion (φ) of both states. As shown in Figure 4C and Table S4, the average lifetimes of State 1 and State 2 (τ_1 and τ_2) gradually decrease with increasing the temperature. Among them, τ_1 decreases from ~34.73 to ~0.06 ms, while τ_2 decreases from ~21.63 to ~0.25 ms. In addition, the higher temperature also facilitates the transition of the molecule to a quasi-planar conformation, as demonstrated by an increase of φ_2 from ~28.6% to ~75.2%. Using the Van't Hoff equation ($-RT\ln K = \Delta H - T\Delta S$), we can deduce the thermodynamic parameters of the C=C bond twisting from the temperature-dependent experiments. Here, we get two fitted lines that intersect at 40 K (Figure 4D). In the higher temperature range, ΔH = 1,010.5 ± 191.7 J mol^{-1} and ΔS = 24.4 ± 3.8 J $mol^{-1}\cdot K^{-1}$. In the lower temperature range,

Please cite this article in press as: Yang et al., Complete deciphering of the dynamic stereostructures of a single aggregation-induced emission molecule, Matter (2022), https://doi.org/10.1016/j.matt.2022.01.016

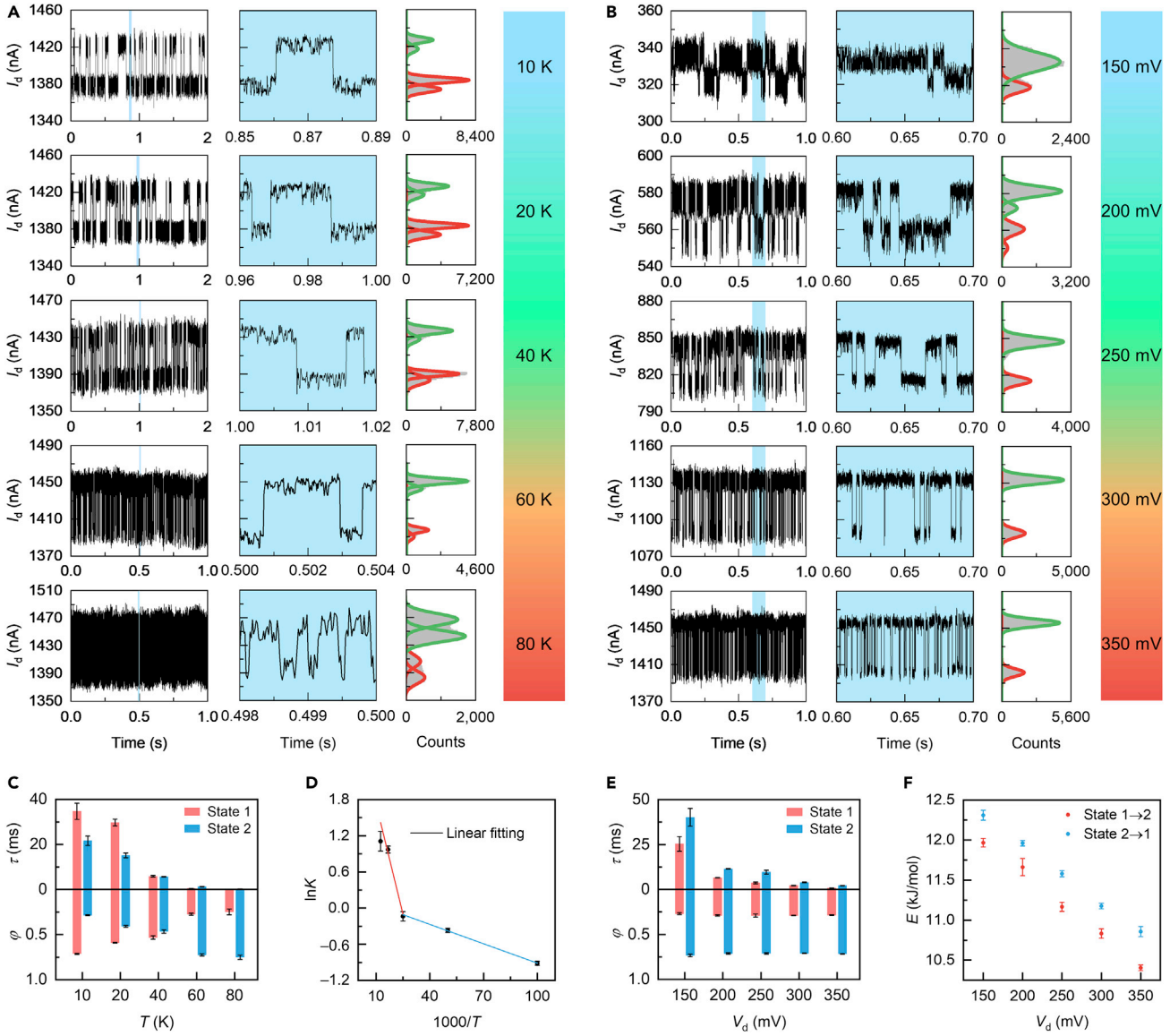

Figure 4. Effects of temperature and electric field on quasi C=C bond twisting

(A and B) *I*–*t* curves, corresponding enlarged *I*–*t* curves marked in blue, and corresponding histograms of the device connected with TPE-2A at different temperatures (A) and bias voltages (B). Data in (A) were obtained at 350 mV, and data in (B) were obtained at 60 K.

(C) Lifetime and occurrence proportion changes of State 1 (red) and State 2 (green) at different temperatures.

(D) Plots of the thermodynamic parameters (ln*K* versus 1,000/*T*) deduced from temperature-dependent measurements. ΔH and ΔS were derived from the Van't Hoff equation.

(E) Lifetime and occurrence proportion changes of State 1 (red) and State 2 (green) at different voltages.

(F) Activation energies for the mutual transformation of States 1 and 2 at different bias voltages. Error bars were calculated from the data obtained from three working devices.

ΔH = 89.0 ± 2.9 J mol^{-1} and ΔS = 1.3 ± 0.2 J mol^{-1}·K^{-1}. We speculate that the underlying reason for this is the confrontation and balance between C=C bond twisting and phenyl rotation. As reported previously,[26] in the ground state and planar conformation, benzene rings of the TPE molecule are more or less locked to a fixed spatial position because of a large steric strain. Under the excitation of electric field, the C=C bond twisting promotes the relaxation of the corresponding

Please cite this article in press as: Yang et al., Complete deciphering of the dynamic stereostructures of a single aggregation-induced emission molecule, Matter (2022), https://doi.org/10.1016/j.matt.2022.01.016

steric strain, and the benzene rings become flexible to rotate. These two transitions influence each other in the process of constantly reaching the next equilibrium point, and the cycle continues. Therefore, the average lifetime (τ_1 and τ_2) derived from this work is not only affected by the C=C bond twisting motion.

Voltage-dependent measurements

We further investigated the effects of different bias voltages, that is, the electric field strength, on the dynamic behavior of C=C bond twisting. We carried out real-time current measurements at different bias voltages ranging from 150 to 350 mV. The obtained $I-t$ curves and the corresponding conductance-based histograms at 60 and 40 K are shown in Figures 4B and S16, respectively. It is clear that, as the bias voltage increases from 150 to 350 mV, φ_1 and φ_2 are almost unchanged, while φ_1 remains at about 71% (Figure 4E). At the same time, the on/off ratios of the conductance switching were calculated to be around 1.05, without obvious dependence on bias voltage. This indicates that the effect of the electric field on the transition energy between the quasi-planar and the perpendicular conformations is almost negligible. However, the derived average lifetimes decrease with increasing the bias voltages (Figures 4E and S17; Table S5), and also with the gradual disappearance of the small current fluctuations. τ_1 decreases from ~25.40 to ~0.85 ms and τ_2 decreases from ~40.20 to ~2.14 ms, suggesting that the electric field can accelerate both C=C bond twisting and the phenyl rotation. According to the Eyring equation, $E = \mathrm{RTln}\left(\frac{k_B T}{hk}\right)$, where R = 8.314 J $mol^{-1}\cdot K^{-1}$, k_B is the Boltzmann constant, and h is the plank constant, the activation energies required for the mutual transformation of States 1 and 2 at different bias voltages can be derived as shown in Figure 4F, again indicating that an electric field can significantly promote the C=C bond twisting by reducing the activation energy. Therefore, it is possible to monitor the rapid intramolecular motion by manipulating the electric field, even without changing the potential energy of each species or state.

Conclusions

This work demonstrates the great potential of using the GMG-SMJ electrical test bed to precisely identify the microscopic stereostructures of individual molecules. We succeeded in visualizing the dynamic process of each unit of a TPE molecule under electric fields, including C=C bond twisting, phenyl rotation, and cyclization. The obtained intramolecular motion characteristics, in combination with ongoing single-molecule luminescence research, is of crucial importance to reveal the intrinsic AIE mechanism and further regulate the single-molecule photophysical properties. Through molecular engineering, by taking advantage of various external control means (such as temperature, electric field, light, magnetic field, and so on), this test bed opens up novel perspectives for the development of future practical functional molecular circuits or sensors. We envisage that further incorporation with ultralow temperature technologies and optical spectroscopies will promote the visualization of the dynamic process at the single-molecule level in multiple dimensions, which would be extremely beneficial to the investigation of the key issues in chemistry and the development of a unique multimodal single-molecule spectroscopic technology.

EXPERIMENTAL PROCEDURES

Resource availability

Lead contact

Further information and requests for resources and reagents should be directed to and will be fulfilled by the lead contact, Xuefeng Guo (Guoxf@pku.edu.cn).

Materials availability

The materials can be produced following the procedures in the section of the synthesis and characterization in the supplemental information.

Data and code availability

This study did not generate any datasets.

SUPPLEMENTAL INFORMATION

Supplemental information can be found online at https://doi.org/10.1016/j.matt.2022.01.016.

ACKNOWLEDGMENTS

We acknowledge primary financial supports from the National Key R&D Program of China (2017YFA0204901, 2021YFA1200101, and 2017YFA0204501), the National Natural Science Foundation of China (22150013, 21727806, 21933001, 22150013, 21788102, 22003030, and 21973099), the Frontiers Science Center for New Organic Matter at Nankai University (63181206), the Natural Science Foundation of Beijing (2222009), and the Tencent Foundation through the XPLORER PRIZE. S.Z. and Z.L. appreciate the support from the High-Performance Computing Platform of the Center for Life Science at Peking University.

AUTHOR CONTRIBUTIONS

X.G., B.Z.T., and A.Q. conceived and designed the experiments. C.Y. fabricated the devices and performed the device measurements. P.S., J.L., and Z.Z. carried out the molecular synthesis. Q.O., Q.P., S.Z., Z.L., and Z.S. built and analyzed the theoretical model and performed the quantum transport calculation. X.G., B.Z.T., A.Q., Z.S., and C.Y. analyzed the data and wrote the paper. All authors discussed the results and commented on the manuscript.

DECLARATION OF INTERESTS

The authors declare no competing interests.

Received: August 13, 2021
Revised: November 11, 2021
Accepted: January 18, 2022
Published: February 8, 2022

REFERENCES

1. Guo, X., Xiang, D., and Li, Y. (2020). Molecular-scale Electronics: Concept, Fabrication and Applications (Wiley-VCH Verlag GmbH & Co).

2. Gehring, P., Thijssen, J.M., and van der Zant, H.S.J. (2019). Single-molecule quantum-transport phenomena in break junctions. Nat. Rev. Phys. *1*, 381–396.

3. Su, T.A., Neupane, M., Steigerwald, M.L., Venkataraman, L., and Nuckolls, C. (2016). Chemical principles of single-molecule electronics. Nat. Rev. Mater. *1*, 16002.

4. Sun, L., Diaz-Fernandez, Y.A., Gschneidtner, T.A., Westerlund, F., Lara-Avila, S., and Moth-Poulsen, K. (2014). Single-molecule electronics: from chemical design to functional devices. Chem. Soc. Rev. *43*, 7378–7411.

5. Xin, N., Guan, J., Zhou, C., Chen, X., Gu, C., Li, Y., Ratner, M.A., Nitzan, A., Stoddart, J.F., and Guo, X. (2019). Concepts in the design and engineering of single-molecule electronic devices. Nat. Rev. Phys. *1*, 211–230.

6. Su, T.A., Li, H., Steigerwald, M.L., Venkataraman, L., and Nuckolls, C. (2015). Stereoelectronic switching in single-molecule junctions. Nat. Chem. *7*, 215–220.

7. Su, T.A., Li, H.X., Klausen, R.S., Kim, N.T., Neupane, M., Leighton, J.L., Steigerwald, M.L., Venkataraman, L., and Nuckolls, C. (2017). Silane and germane molecular electronics. Acc. Chem. Res. *50*, 1088–1095.

8. Venkataraman, L., Klare, J.E., Nuckolls, C., Hybertsen, M.S., and Steigerwald, M.L. (2006). Dependence of single-molecule junction conductance on molecular conformation. Nature *442*, 904–907.

9. Diez-Perez, I., Hihath, J., Hines, T., Wang, Z.-S., Zhou, G., Müllen, K., and Tao, N. (2011). Controlling single-molecule conductance through lateral coupling of π orbitals. Nat. Nanotechnol. *6*, 226–231.

10. Guo, X. (2020). Molecular engineering: a key route to improve the performance of molecular devices. Matter *2*, 284–285.

11. Schwarz, F., Kastlunger, G., Lissel, F., Egler-Lucas, C., Semenov, S.N., Venkatesan, K., Berke, H., Stadler, R., and Loertscher, E. (2016). Field-induced conductance switching by charge-state alternation in organometallic single-molecule junctions. Nat. Nanotechnol. *11*, 170–176.

12. Nacci, C., Foelsch, S., Zenlchowski, K., Dokic, J., Klamroth, T., and Saalfrank, P. (2009). Current versus temperature-induced switching in a single-molecule tunnel junction: 1,5 cyclooctadiene on Si(001). Nano Lett. *9*, 2996–3000.

13. Tomasz, M., Bogdana, B., Rémi, P., Verena, S., Marcel, P., Ivan, P., Ulrike, K., Hagen, K., Peter, W., Pingo, M., et al. (2020). Controlling single molecule conductance by a locally induced chemical reaction on individual thiophene units. Angew. Chem. Int. Ed. *59*, 6207–6212.

14. Jia, C., Wang, J., Yao, C., Cao, Y., Zhong, Y., Liu, Z., Liu, Z., and Guo, X. (2013). Conductance switching and mechanisms in single-molecule junctions. Angew. Chem. Int. Ed. *52*, 8666–8670.

15. Dulić, D., van der Molen, S.J., Kudernac, T., Jonkman, H.T., de Jong, J.J.D., Bowden, T.N., van Esch, J., Feringa, B.L., and van Wees, B.J. (2003). One-way optoelectronic switching of photochromic molecules on gold. Phys. Rev. Lett. *91*, 207402.

16. Meng, L., Xin, N., Hu, C., Wang, J., Gui, B., Shi, J., Wang, C., Shen, C., Zhang, G., Guo, H., et al. (2019). Side-group chemical gating via reversible optical and electric control in a single molecule transistor. Nat. Commun. *10*, 1450.

17. Kumagai, T., Hanke, F., Gawinkowski, S., Sharp, J., Kotsis, K., Waluk, J., Persson, M., and Grill, L. (2014). Controlling intramolecular hydrogen transfer in a porphycene molecule with single atoms or molecules located nearby. Nat. Chem. *6*, 41–46.

18. Doppagne, B., Neuman, T., Soria-Martinez, R., López, L.E.P., Bulou, H., Romeo, M., Berciaud, S., Scheurer, F., Aizpurua, J., and Schull, G. (2020). Single-molecule tautomerization tracking through space- and time-resolved fluorescence spectroscopy. Nat. Nanotechnol. *15*, 207–211.

19. Jia, C., Migliore, A., Xin, N., Huang, S., Wang, J., Yang, Q., Wang, S., Chen, H., Wang, D., Feng, B., et al. (2016). Covalently bonded single-molecule junctions with stable and reversible photoswitched conductivity. Science *352*, 1443–1445.

20. Donhauser, Z.J., Mantooth, B.A., Kelly, K.F., Bumm, L.A., Monnell, J.D., Stapleton, J.J., Price, D.W., Rawlett, A.M., Allara, D.L., Tour, J.M., et al. (2001). Conductance switching in single molecules through conformational changes. Science *292*, 2303–2307.

21. Zhang, J., Zhong, J., Lin, J., Hu, W., Wu, K., Xu, G., Wee, A.T.S., and Chen, W. (2015). Towards single molecule switches. Chem. Soc. Rev. *44*, 2998–3022.

22. Metzger, R.M. (2015). Unimolecular electronics. Chem. Rev. *115*, 5056–5115.

23. Garner, M.H., Li, H., Chen, Y., Su, T.A., Shangguan, Z., Paley, D.W., Liu, T., Ng, F., Li, H., Xiao, S., et al. (2018). Comprehensive suppression of single-molecule conductance using destructive σ-interference. Nature *558*, 415–419.

24. Bai, J., Daaoub, A., Sangtarash, S., Li, X., Tang, Y., Zou, Q., Sadeghi, H., Liu, S., Huang, X., Tan, Z., et al. (2019). Anti-resonance features of destructive quantum interference in single-molecule thiophene junctions achieved by electrochemical gating. Nat. Mater. *18*, 364–369.

25. Li, Y., Buerkle, M., Li, G., Rostamian, A., Wang, H., Wang, Z., Bowler, D.R., Miyazaki, T., Xiang, L., Asai, Y., et al. (2019). Gate controlling of quantum interference and direct observation of anti-resonancesin single molecule charge transport. Nat. Mater. *18*, 357–363.

26. Lenderink, E., Duppen, K., and Wiersma, D.A. (1995). Femtosecond twisting and coherent vibrational motion in the excited state of tetraphenylethylene. J. Phys. Chem. *99*, 8972–8977.

27. Barbara, P.F., Rand, S.D., and Rentzepis, P.M. (1981). Direct measurements of tetraphenylethylene torsional motion by picosecond spectroscopy. J. Am. Chem. Soc. *103*, 2156–2162.

28. Henson, A.B., Gersten, S., Shagam, Y., Narevicius, J., and Narevicius, E. (2012). Observation of resonances in penning ionization reactions at sub-Kelvin temperatures in merged beams. Science *338*, 234–238.

29. Hu, M., Liu, Y., Grimes, D.D., Lin, Y.-W., Gheorghe, A.H., Vexiau, R., Bouloufa-Maafa, N., Dulieu, O., Rosenband, T., and Ni, K. (2019). Direct observation of bimolecular reactions of ultracold KRb molecules. Science *366*, 1111–1115.

30. Yang, H., Zhang, D., Liu, L., Liu, Y., Nan, J., Zhao, B., and Pan, J. (2019). Observation of magnetically tunable Feshbach resonances in ultracold (NaK)-Na-23-K-40+K-40 collisions. Science *363*, 261–264.

31. Zhao, Z., Zhang, H., Lam, J.W.Y., and Tang, B.Z. (2020). Aggregation-induced emission: new vistas at aggregate level. Angew. Chem. Int. Ed. *59*, 9888–9907.

32. Hong, Y., Lam, J.W.Y., and Tang, B.Z. (2011). Aggregation-induced emission. Chem. Soc. Rev. *40*, 5361–5388.

33. Cai, Y., Du, L., Samedov, K., Gu, X., Qi, F., Sung, H.H.Y., Patrick, B.O., Yan, Z., Jiang, X., Zhang, H., et al. (2018). Deciphering the working mechanism of aggregation-induced emission of tetraphenylethylene derivatives by ultrafast spectroscopy. Chem. Sci. *9*, 4662–4670.

34. Shustova, N.B., Ong, T.C., Cozzolino, A.F., Michaelis, V.K., Griffin, R.G., and Dinca, M. (2012). Phenyl ring dynamics in a tetraphenylethylene-bridged metal-organic framework: implications for the mechanism of aggregation-induced emission. J. Am. Chem. Soc. *134*, 15061–15070.

35. Leung, N.L.C., Xie, N., Yuan, W., Liu, Y., Wu, Q., Peng, Q., Miao, Q., Lam, J.W.Y., and Tang, B.Z. (2014). Restriction of intramolecular motions: the general mechanism behind aggregation-induced emission. Chem. Eur. J. *20*, 15349–15353.

36. Xin, N., Wang, J., Jia, C., Liu, Z., Zhang, X., Yu, C., Li, M., Wang, S., Gong, Y., Sun, H., et al. (2017). Stereoelectronic effect-induced conductance switching in aromatic chain single-molecule junctions. Nano Lett. *17*, 856–861.

37. Song, H., Kim, Y., Jang, Y.H., Jeong, H., Reed, M.A., and Lee, T. (2009). Observation of molecular orbital gating. Nature *462*, 1039–1043.

38. Wang, W., Lee, T., Kretzschmar, I., and Reed, M.A. (2004). Inelastic electron tunneling spectroscopy of an alkanedithiol self-assembled monolayer. Nano Lett. *4*, 643–646.

39. Li, Y., Yang, C., and Guo, X. (2020). Single-molecule electrical detection: a promising route toward the fundamental limits of chemistry and life science. Acc. Chem. Res. *53*, 159–169.

40. Baldo, M.A., O'Brien, D.F., Tompson, M.E., and Forrest, S.R. (1999). Excitonic singlet–triplet ratio in a semiconducting organic thin film. Phys. Rev. B *60*, 14422–14428.

41. Shao, Y., Head-Gordon, M., and Krylov, A.I. (2003). The spin–flip approach within time-dependent density functional theory: theory and applications to diradicals. J. Chem. Phys. *118*, 4807–4818.

42. Tran, T., Prlj, A., Lin, K., Hollas, D., and Corminboeuf, C. (2019). Mechanisms of fluorescence quenching in prototypical aggregation-induced emission systems: excited state dynamics with TD-DFTB. Phys. Chem. Chem. Phys. *21*, 9026–9035.